Electronic Supplementary Material (ESI) for ChemComm.

Supplemental Information

Sn_{36}^{8-}: A 2.7 nm Naked Aromatic Tin Rod

Nikolay V. Tkachenko, Wei-Xing Chen, Harry W. T. Morgan, Alvaro Muñoz-Castro, Alexander I. Boldyrev, and Zhong-Ming Sun

Supplemental Information

Table of Contents

Supplemental Experimental Procedures

1. Experimental Procedures

General experimental considerations: All manipulations and reactions were performed under a nitrogen atmosphere using standard Schlenk or glovebox techniques. Ethylenediamine (en) (Aldrich, 99%) and DMF (Aldrich, 99.8%) were freshly distilled by CaH_2 prior to use, and stored in N_2 prior to use. Tol (Aldrich, 99.8%) was distilled from sodium/benzophenone under nitrogen and stored under nitrogen. 2.2.2-crypt (4,7,13,16,21,24-Hexaoxa-1,10-diazabicyclo (8.8.8) hexacosane, purchased from Sigma-Aldirich, 98%) was dried in vacuum for one day prior to use. K_4Sn_9 was synthesized by heating a stoichiometric mixture of the elements (K: +99 %, Sn: 99.99 % all from Aladdin) at 850 °C for two days in a niobium tube. $Na[Zn(Cp)_3]$ was prepared according to literature methodology.[1]

Synthesis of $[K(2,2,2\text{-crypt})]_8[Sn_{36}]$ (1):

K_4Sn_9 (0.1 mmol) and 2.2.2-crypt (150mg, 0.4 mmol) were dissolved in en (ca. 3 mL) and stirred for 30 min, resulting a dark brown solution. Then $Na[Zn(Cp)_3]$ (33 mg, 0.15 mmol) was dispersed in toluene (0.5 mL), producing a light pink suspension, and then added dropwise to the above mixture. After stirring for 3 hours at room temperature, the resulting brown solution was filtered through glass wool and transferred to a test tube, then carefully layered by toluene (ca. 3 mL) to allow for crystallization. Small green block-like crystals of **1** (16 mg, 13% yield based on the used precursor K_4Sn_9) were isolated after two weeks.

X-ray Diffraction:

Suitable single crystals were selected for X-ray diffraction analyses. Crystallographic data were collected on Rigaku XtalAB Pro MM007 DW diffractometer with graphite monochromated Cu Kα radiation (λ = 1.54184 Å).

Electrospray Ionization Mass Spectrometry (ESI-MS) Investigations:

Negative ion mode ESI-MS of the DMF solutions of the single crystal and reaction solution were measured on an LTQ linear ion trap spectrometer by Agilent Technologies ESI-TOF-MS (6230). The spray voltage was 5.48 kV and the capillary temperature was kept at 300 °C. The capillary voltage was 30 V. The samples were made up inside a glovebox under a nitrogen atmosphere and rapidly transferred to the spectrometer in an airtight syringe by direct infusion with a Harvard syringe pump at 0.2 mL/ min.

Energy Dispersive X-ray (EDX) Spectroscopic Analysis:

EDX analysis on the title clusters were performed using a scanning electron microscope (FE-SEM, JEOL JSM-7800F, Japan). Data acquisition was performed with an acceleration voltage of 15 kV and an accumulation time of 60 s.

2. Crystallographic details

Structure was solved using direct methods and then refined using SHELXL-2014 and Olex2[2-4] to convergence, in which all the non-hydrogen atoms were refined anisotropically during the final cycles. All hydrogen atoms of the organic molecule were placed by geometrical considerations and were added to the structure factor calculation. We used the PLATON SQUEEZE procedure[5] to remove the solvent molecules which could not be modeled properly. For compound **1**, the 2.2.2-crypt molecules have a relatively large tendency to disorder, we performed disorder processing and required the application of restraints to this large number of atoms (the alternative application of the back-Fourier-transform method did not produce more reliable results). As a results, we refined the structure by using some requisite restrains of anisotropy, such as SIMU, DFIX for the K-crypt fragments and omitting the most disagreeable reflections. The crystal data of **1** was collected under nitrogen conditions at 100K. A summary of the crystallographic data for the title compounds was listed in Table S1, and selected bond distances were given in Table S2. CCDC entry 2086696 for compound **1** contain the supplementary crystallographic data for this paper. These data can be obtained free of charge from The Cambridge Crystallographic Data Centre (www.ccdc.cam.ac.uk/data_request/cif).

Table S1. X-ray measurements and structure solutions of $[K(2,2,2\text{-crypt})]_8[Sn_{36}]$ (**1**).

Compound	**1**
CCDC number	2086696
Empirical formula	$C_{71.04}H_{133.07}K_4N_8O_{24}Sn_{18}$
Formula weight	3776.22
Temperature/K	100
Crystal system	triclinic
Space group	*P*-1
a /Å	15.2975(3)
b /Å	17.9538(3)
c /Å	23.1279(5)
α/°	85.023(2)
β/°	85.230(2)
γ/°	75.808(2)
V /Å^3	6122.3(2)
Z	2
ρ_{calc} /g·cm^{-3}	2.048
$\mu(Cu_{K\alpha})$ /mm^{-1}	30.301
F(000)	3567.0
2Θ range /°	6.856 to 132
Reflections collected / unique	60010 / 20484
Data / restraints / parameters	20484 / 5909 / 1262
R_1/wR_2 (I>2σ(I))[a]	0.0885; 0.2134
R_1/wR_2 (all data)	0.1243; 0.2418
GooF (all data)[b]	0.956
Max. peak/hole /e$^-$·Å^{-3}	2.77 / -1.60

[a] $R_1 = = \sum||F_o|-|F_c||/\sum|F_o|$; $wR_2 = \{\sum w[(F_o)^2-(F_c)^2]^2/\sum w[(F_o)^2]^2\}^{1/2}$

[b] GooF = $\{\sum w[(Fo)^2-(Fc)^2]^2/(n-p)\}^{1/2}$

Table S2. Selected bond distances (Å) for the major components of **1**.

Cluster		Sn_{36}^{8-}	
Sn1-Sn2	3.0425(18)	Sn9-Sn12	3.2234(16)
Sn1-Sn3	2.9668(16)	Sn10-Sn11	3.1049(13)
Sn1-Sn4	2.974(2)	Sn10-Sn12	3.0055(12)
Sn1-Sn5	3.0230(17)	Sn10-Sn13	2.9666(14)
Sn1-Sn7	3.2939(16)	Sn10-Sn18'	2.9755(13)
Sn2-Sn3	3.0620(19)	Sn11-Sn12	3.0987(14)
Sn2-Sn4	2.9427(16)	Sn11-Sn13	2.9505(13)
Sn2-Sn6	2.9539(16)	Sn11-Sn16'	2.9675(11)
Sn2-Sn8	3.2125(18)	Sn11-Sn17'	3.1896(13)
Sn3-Sn5	2.9962(18)	Sn12-Sn16'	3.0277(15)
Sn3-Sn6	2.9494(17)	Sn12-Sn18'	3.0805(16)
Sn4-Sn7	2.8846(17)	Sn13-Sn14	2.9169(13)
Sn4-Sn8	3.0133(17)	Sn13-Sn17'	3.0242(12)
Sn5-Sn7	2.8798(18)	Sn14-Sn15	2.9200(13)
Sn5-Sn9	2.9475(15)	Sn14-Sn15'	2.9907(11)
Sn6-Sn8	2.9560(17)	Sn14-Sn17'	3.0375(14)
Sn6-Sn9	2.9325(16)	Sn14-Sn18'	2.9372(16)
Sn6-Sn10	3.0556(9)	Sn15-Sn16	2.9052(13)
Sn7-Sn8	3.0736(15)	Sn15-Sn17	3.0786(14)
Sn7-Sn9	3.0208(14)	Sn15-Sn18	2.9327(13)
Sn7-Sn10	2.9910(14)	Sn16-Sn17	2.9896(13)
Sn8-Sn9	3.1183(19)	/	/

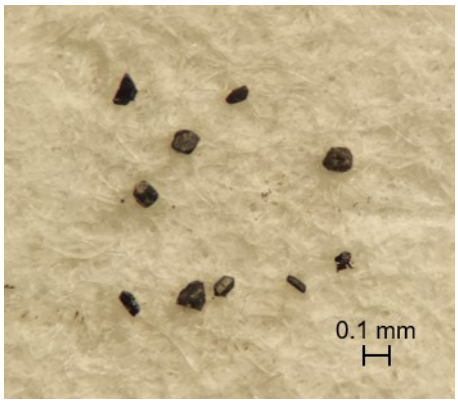

Figure S1. Crystal image of **1**.

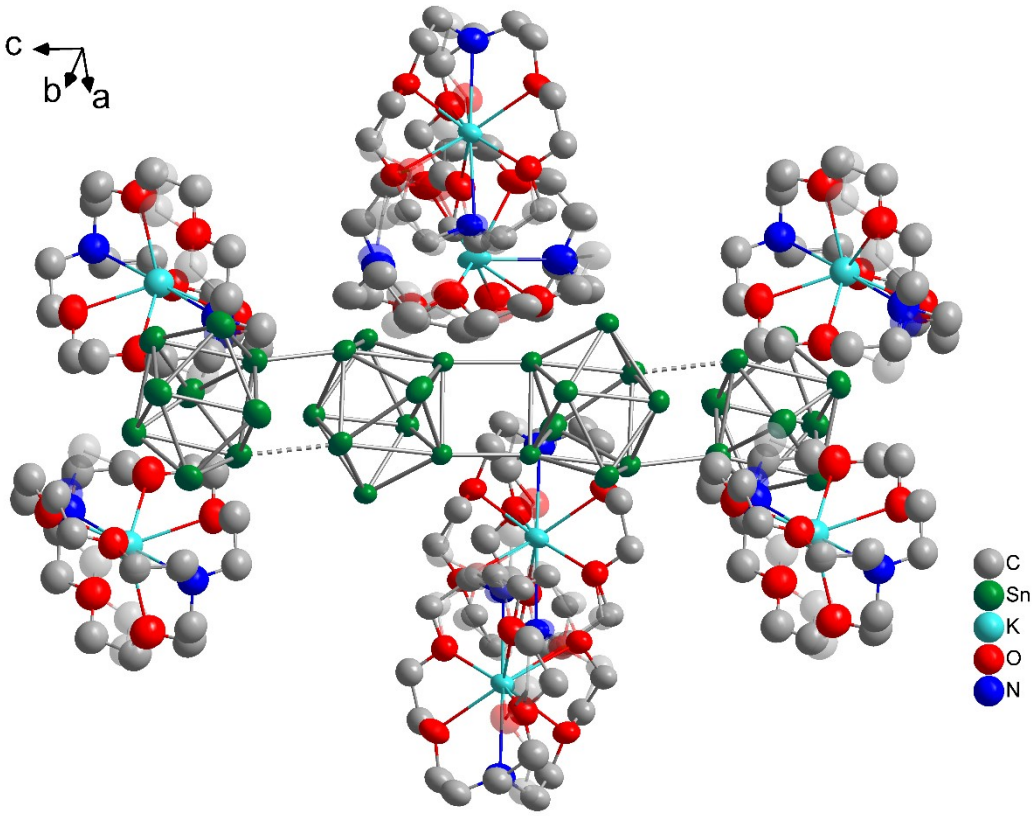

Figure S2. Asymmetric unit of **1**. The disordered part is set to 50% transparency.

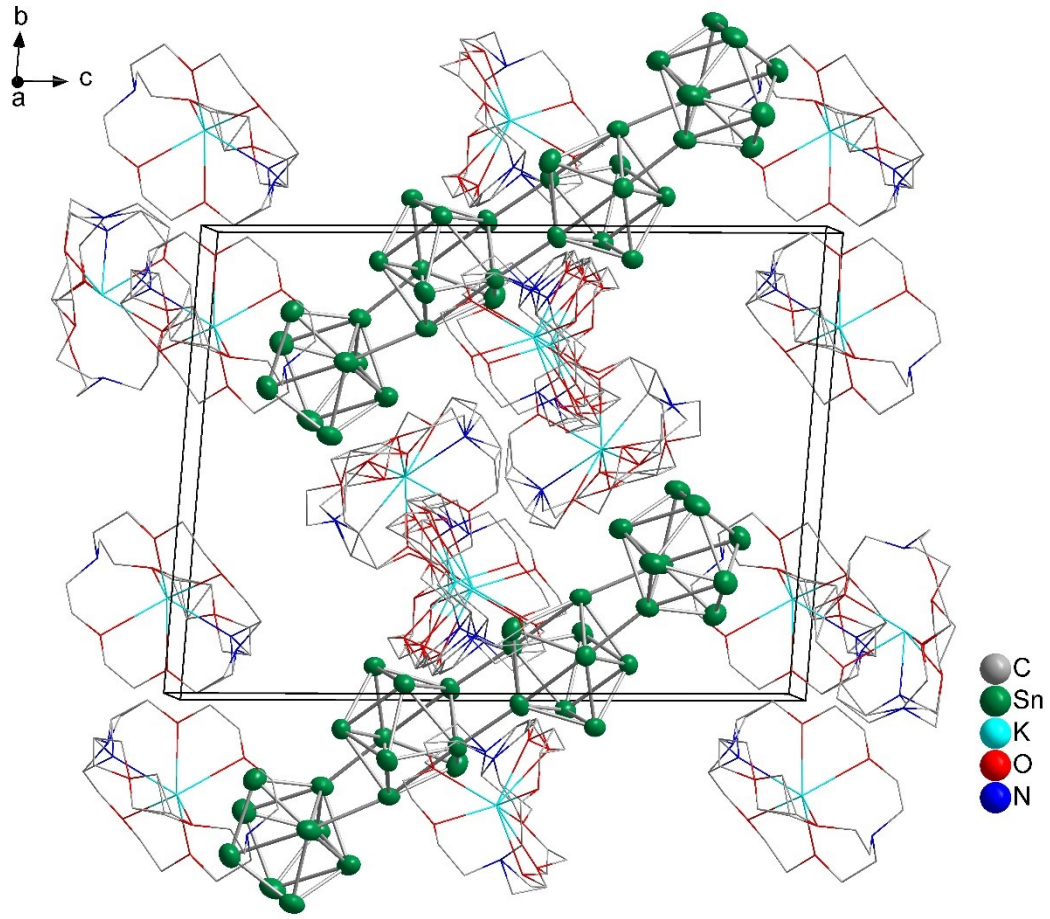

Figure S3. Unit cell of **1**. Minor component in the cluster site are omitted for clarity.

3. ESI-MS Studies

The ESI-MS of the DMF solution of the crystals of **1** failed to obtain the signal of parent cluster anion $[Sn_{36}]^-$ but only $[K(2,2,2\text{-crypt})Sn_9]^-$ (m/z = 1484.3451) fragment was detected (weak). This indicated that **1** underwent fast decomposition during the experiments (Figure S4). Measured and simulated isotope distributions of the detected fragment was shown in the Figure S5.

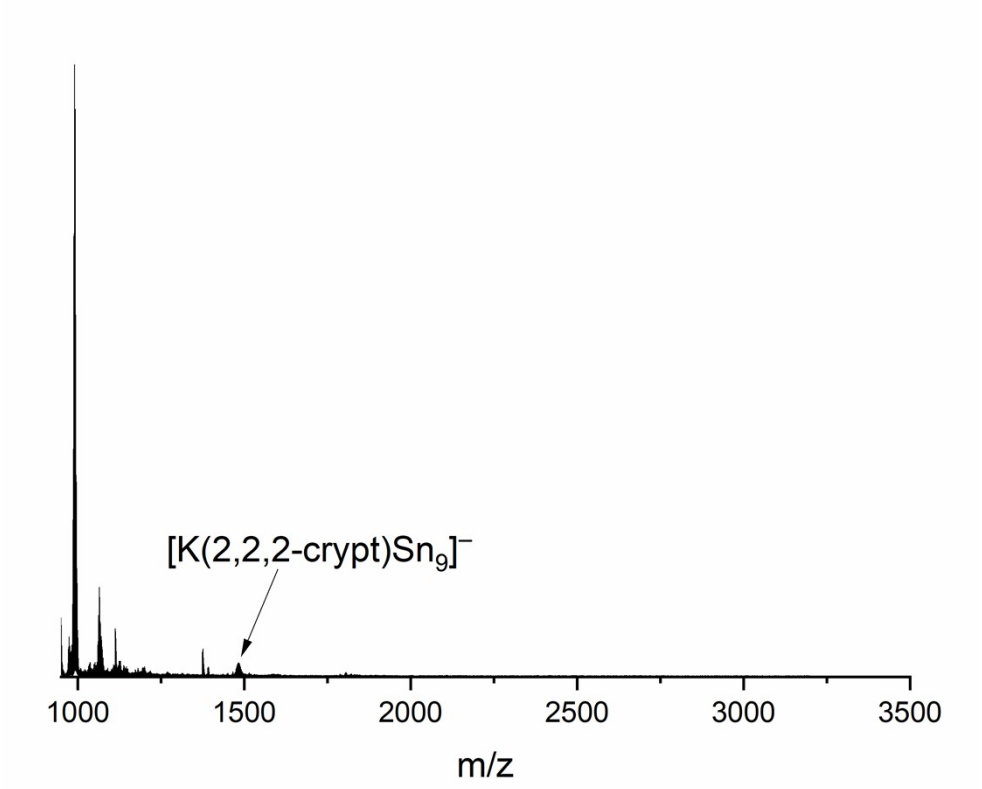

Figure S4. Overview ESI mass spectrum in negative ion mode recorded immediately upon injection of a fresh DMF solution of $[K(2,2,2\text{-crypt})]_8[Sn_{36}]$ (**1**).

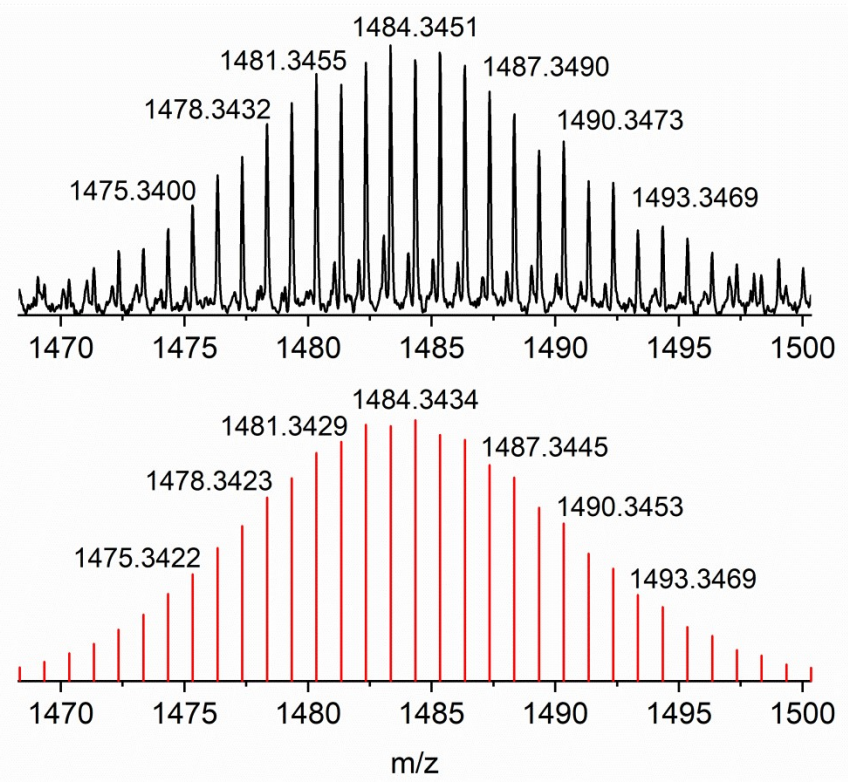

Figure S5. Measured (top) and simulated (bottom) spectrum of the fragment $[K(2,2,2\text{-crypt})Sn_9]^-$.

4. Energy Dispersive X-ray (EDX) Spectroscopic Analysis

EDX analysis on **1** (Figure S6) was performed by a scanning electron microscope (FE-SEM, JEOL JSM-7800F, Japan). Data acquisition was performed with an acceleration voltage of 15 kV and an accumulation time of 60 s. The atomic ratios of K/Sn in complexes **1** is 10.5:36. A deviation in quantity K was observed in the EDX representation, which may be due to the irregular surface of a crystals after exposure to air.

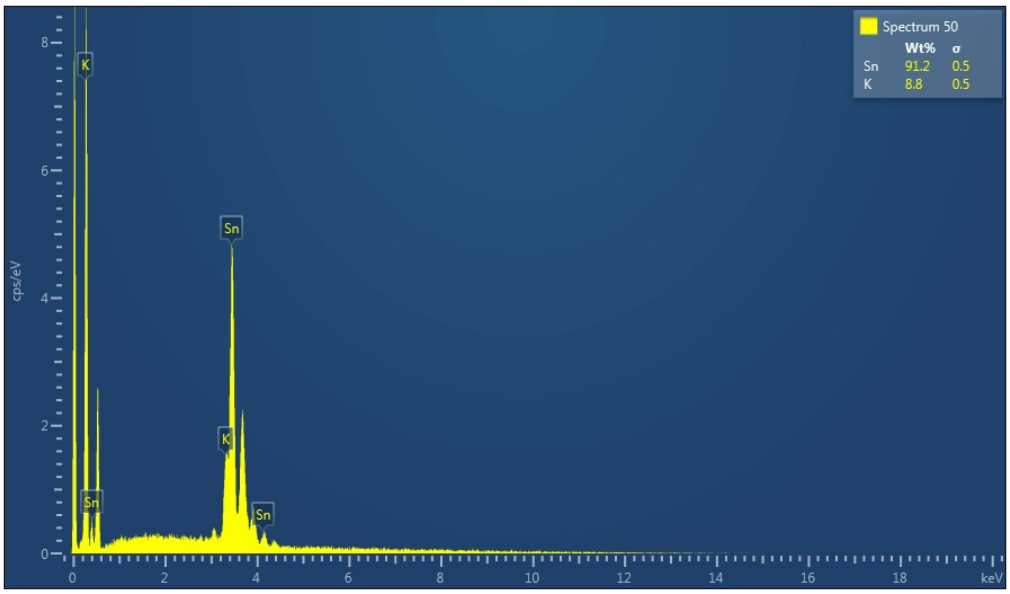

Figure S6. EDX analysis of $[K(2,2,2\text{-crypt})]_8[Sn_{36}]$.

Element	Line type	wt%	σ	Observed / Calculated Element Ratio
K	K series	8.8	0.5	10.5/8.0
Sn	L series	91.2	0.5	36.0/36.0

5. Computational Details.

Quantum chemical methods.

Chemical Bonding analysis: All model clusters were optimized at the DFT level using the PBE0[6] hybrid density functional and def2-TZVP basis set.[7] The Gaussian 16 code[8] was used for the optimization procedures. The same level was used for the adaptive natural density partitioning (AdNDP) analysis performed via AdNDP 2.0 code,[9,10] and electron localization function (ELF) analysis performed using the Multiwfn program.[11,12] To determine chemical bonding pattern for large synthesized structures Sn_{36}^{8-}, we performed a single-point calculation at the same level of theory at the geometry obtained from the X-Ray experiment and at the optimized geometry. The frequency calculations were performed using the harmonic approximation. The dissociation energies were calculated as a difference in energy between dissociated optimized clusters and the tetramer with ZPE corrections. The level of theory was PBE0/def2-TZVP. The isolated negatively charged species are unstable toward electron emission and possess positive energies of occupied KS-orbitals. To stabilize the highly negative charge we used the CPCM solvent model, in order to make the clusters stable toward the electron detachment.

Magnetic response analysis: Geometry optimizations and subsequent calculations were performed using scalar relativistic DFT methods employing the ADF code[13] with the all-electron triple-ζ Slater basis set plus the double-polarization (STO-TZ2P) basis set in conjunction with the PBE0 functional.[6,14] Relativistic effects were considered through the ZORA Hamiltonian.[23] The nucleus-independent shielding tensors (σ_{ij})[15-18] were calculated within the GIAO formalism, employing the OPBE[14,18,19] functional and an all-electron STO-TZ2P basis set, placed in a three-dimensional grid in order to evaluate the induced field ($\mathbf{B}^{ind}$), upon an external magnetic field ($\mathbf{B}^{ext}$) at the molecular surroundings, related via $B_i^{ind} = -\sigma_{ij}B_j^{ext}$.[15,17,20-22] For convenience, the *i* and *j* suffixes are related to the x-, y- and z-axes of the molecule-fixed Cartesian system (*i*,*j* = x,y,z). The values of B^{ind} are given in ppm in relation to B^{ext}.

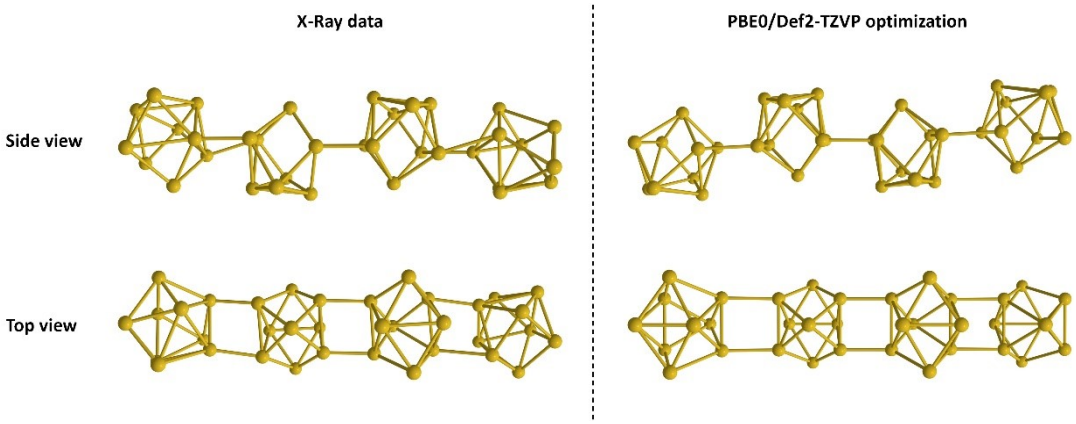

Figure S7. Structures of Sn_{36}^{8-} obtained from X-ray data (left) and DFT calculations (right)

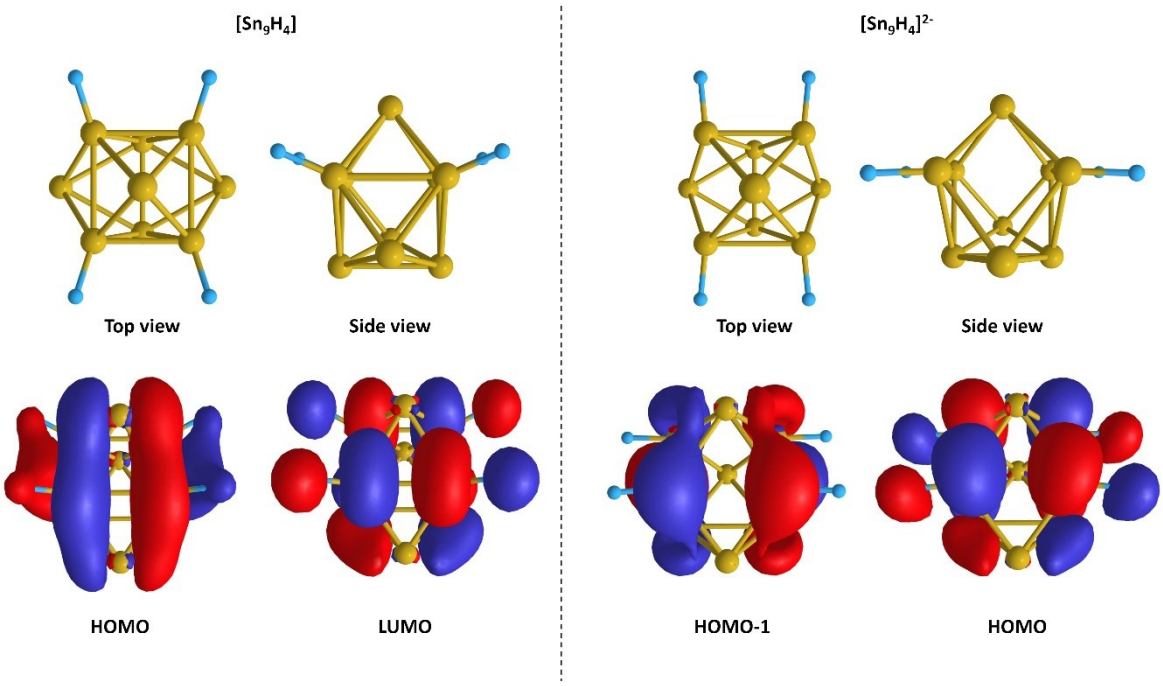

Figure S8. Illustration of optimized structures (top) and selected molecular orbitals (bottom) of $[Sn_9H_4]$ (left) and $[Sn_9H_4]^{2-}$ (right).

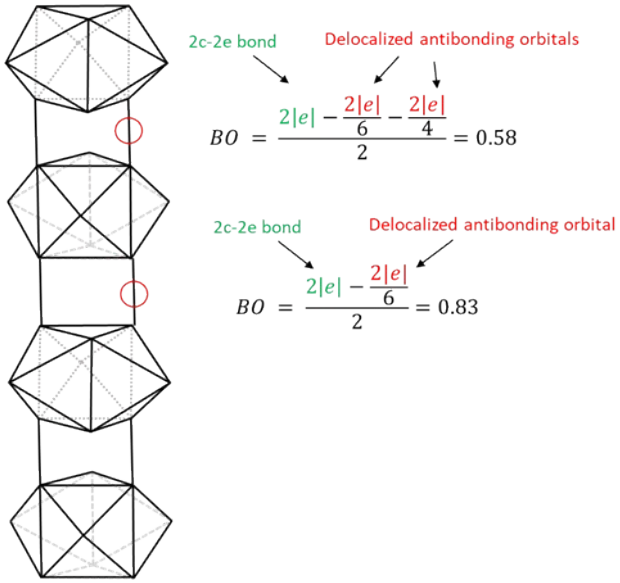

Figure S9. Calculation of formal bond order based on the AdNDP analysis.

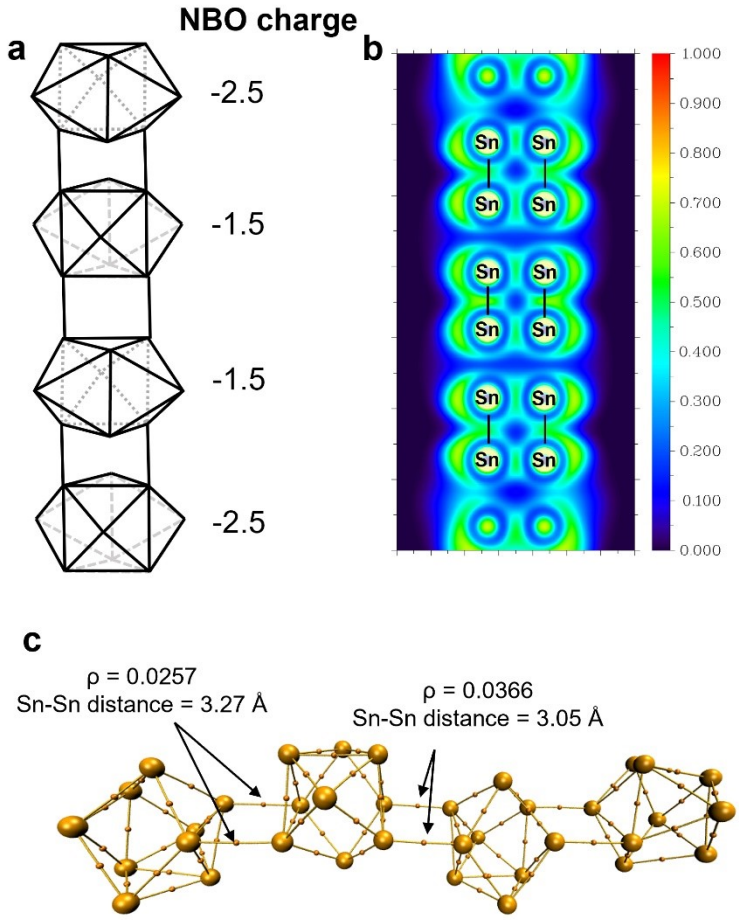

Figure S10. (a) Natural charge of each Sn_9 fragment; (b) ELF-plot of Sn_{36}^{8-} cluster in the plane of Sn-Sn inter-cluster bonds; (c) Bond paths and bond critical points of Sn_{36}^{8-} cluster obtained via QTAIM analysis.

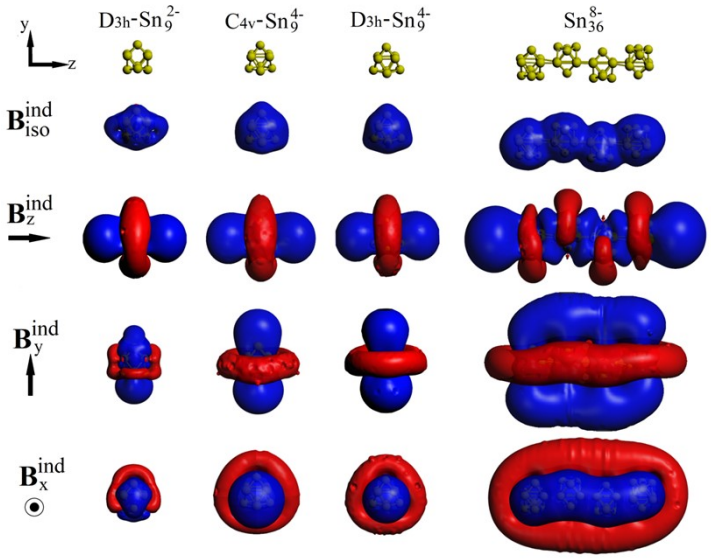

Figure S11. Magnetic response properties of D_{3h}-Sn_9^{2-}, C_{4v}-Sn_9^{4-}, D_{3h}-Sn_9^{4-}, and, Sn_{36}^{8-}, given by isotropic term (B^{ind}_{iso}), and, specific orientations of the external field (B^{ind}_{z}, B^{ind}_{x}, and B^{ind}_{y}). Isosurfaces at ±3.0 ppm; Blue: shielding; Red: deshielding.

Sn_9 units parallel bonding and bond order analysis of Sn_{36}^{8-}: To illustrate that the coupling between Sn_9 units in a parallel manner is impossible without those antibonding elements, we performed model calculations on $[Sn_9H_4]$ and $[Sn_9H_4]^{2-}$ species. Those clusters are not thermodynamically stable, but the behavior of electron density in such clusters can nevertheless provide some insights. The optimized geometry of the Sn_9 fragment in neutral $[Sn_9H_4]$ almost perfectly conserves the D_{3h} symmetry, while the hydrogen-tin bonds are directed radially from the cluster (Figure S8). In turn, with the addition of two extra electrons, the optimized structure changes. We observe an elongation of Sn–Sn bonds within the cluster and elongation of Sn–H bonds. Moreover, the direction of Sn–H bonds changes, showing the same parallel arrangement observed in Sn_{36}^{8-} (Figure S8). The comparison of HOMO and LUMO orbitals of $[Sn_9H_4]$ with HOMO-1 and HOMO orbitals of $[Sn_9H_4]^{2-}$ indicates that the extra two electrons occupy a delocalized orbital with antibonding character (Figure S8). Similar behavior was described in previous works by Sevov and coworkers in Ge assembled polymers.[26,27] Thus, the presence of additional two electrons on the anti-bonding orbital is crucial to the correct direction of 2c-2e bonds. Without this alignment, the tetramerization of Sn_9 fragments is geometrically inhibited.

Due to the presence of two delocalized anti-bonding elements, the bond order of Sn–Sn 2c-2e bond is less than one. In Figure S9, we show the calculations of formal bond orders for central Sn–Sn bonds and terminal Sn–Sn bonds. We observe that the formal bond orders of the central 2c-2e bonds are higher than the terminal ones which is reflected in the shorter bond distances in the optimized structure (3.05 Å for central Sn–Sn *vs* 3.27 Å for terminal Sn–Sn bonds). The antibonding character of the delocalized bonds is responsible for Sn–Sn distance elongation within each quasi-D_{3h} symmetric Sn_9 fragment. The bond orders calculated within AdNDP are in good agreement with the calculated Wiberg bond orders (WBO = 0.83 for central Sn–Sn; WBO = 0.66 for terminal Sn–Sn)[28] and the quantum theory of atoms in molecules (QTAIM)[29] delocalization indices (DI = 0.68 for central Sn–Sn; DI = 0.46 for terminal Sn–Sn). Additionally, the dissociation energies confirm the stronger interaction between central Sn_9 units than between the terminal and the central fragments. Thus, the following dissociation energies were obtained: 20.2 kcal/mol for the dissociation of terminal Sn_9^{2-} from Sn_{27}^{6-} and 30.7 kcal/mol for the dissociation of the tetramer into two Sn_{18}^{4-} dimers. Analysis of the electron localization function (ELF)[11] and QTAIM analysis are consistent with the AdNDP description, showing electron localization regions in the space between Sn_9 fragments (Figure S10). The analysis of natural charge density showed a slightly more negative charge of terminal Sn_9 units. This can be explained with the different bonding schemes for two central Sn_9 units and two terminal units. The central units participate in four Sn-Sn 2c-2e σ-bonds while the outer Sn_9 clusters possess only two 2c-2e bonds and extra two s-type lone pairs. Due to the presence of those lone pairs, the outer units have slightly more negative charge. We note, this difference in natural charge does not affect the aromatic properties of each Sn_9 fragment since it is a consequence of different inter-cluster bonding regimes.

Sn_{36}^{8-} as molecular wires. Electronic communication is a relevant issue towards the formation of molecular wires.[24] The Sn_{36}^{8-} cluster and its Ge_{36}^{8-} counterpart were evaluated in terms of electronic communication between each E_9 unit (E=Ge, Sn) via broken symmetry[25] calculations for both mono-oxidized (E_{36}^{7-}) and mono-reduced (E_{36}^{9-}) counterparts. This approach enables to locate the unpaired electron initially in each E_9 unit in order to treat such units as distinct redox centers, and hence, evaluate qualitatively further electron communication along with the whole cluster in the resulting spin-density (spin-density = ρ_α - ρ_β). The obtained results show that independent from the location of the unpaired electron in both mono-oxidized (E_{36}^{7-}) and mono-reduced (E_{36}^{9-}) species, which varies from the first to the last E_9 unit from left to right as denoted by the vertical black arrow in Figure S12, a full delocalization of the unpaired electron is achieved, as denoted by the spread electron density along the whole cluster backbone for both Sn_{36}^{8-} and Ge_{36}^{8-} in their

mono-oxidized and mono-reduced forms supporting their view as models for molecular wires from Zintl-ion clusters.

For broken symmetry calculations, geometry optimizations have been done within the unrestricted DFT formalism at the same level of theory of other calculations from this manuscript, with a modified unsymmetrical starting potential which initially localizes the unpaired electron on one E atom from each E_9 unit, which requires neglect any symmetry operations (i.e., no symmetry), in order to treat each redox E_9 unit independently. For all the calculations, the final self-consistent field (SCF) to achieve the final electron density exhibits a full delocalized paramagnetic system, with the unpaired electron distributed in near the same proportion on the different E_9 units (Figure S12).

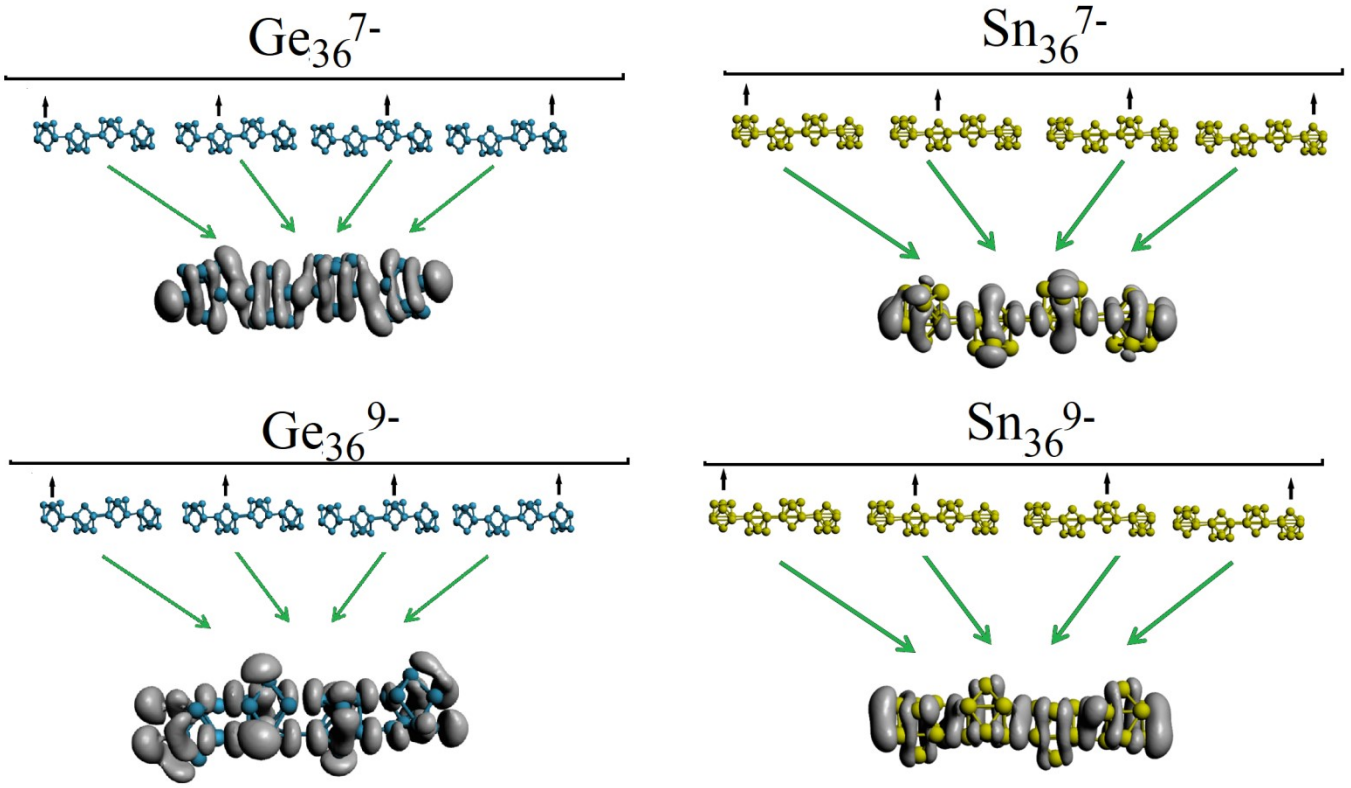

Figure S12. Spin-density for E_{36}^{7-} and E_{36}^{9-} (E=Ge, Sn), obtained from broken symmetry calculations.

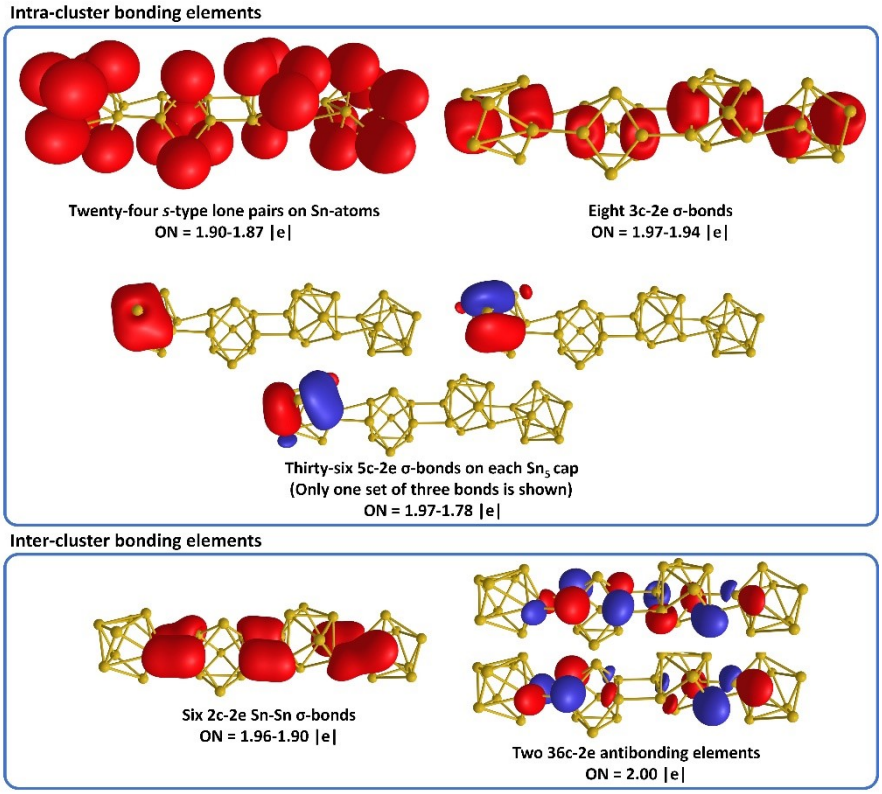

Figure S13. Chemical bonding pattern of Sn_{36}^{8-} cluster at a non-optimized geometry obtained from the X-ray analysis. Different phases of a bonding element are represented with different colors. Lines between atoms are presented for visualization and do not necessarily correspond to 2c-2e bonds.

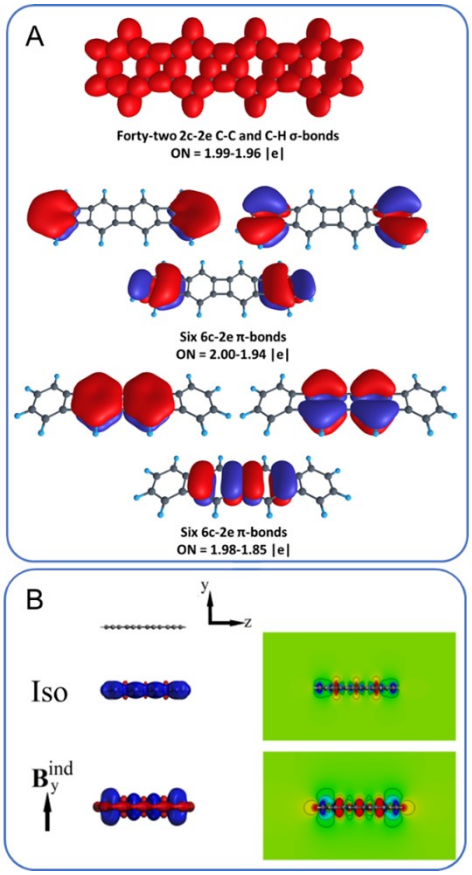

Figure S14. (A) Chemical bonding pattern of $C_{24}H_{12}$ obtained from AdNDP analysis. Different phases of the bonding element are represented with different colors. (B) Magnetic response properties of $C_{24}H_{12}$, given by isotropic term (Iso), and specific orientations of the external field (B^{ind}_y). Isosurfaces at ±3.0 ppm; Blue: shielding; Red: deshielding.

Table S3. Cartesian coordinates of optimized Sn_{36}^{8-} cluster.

Sn_{36}^{8-}	Level of theory: PBE0/def2-TZVP			
	50	1.489697000	0.314797000	-1.509876000
	50	-1.560581000	0.279039000	-1.442089000
	50	-5.071307000	2.316430000	0.587936000
	50	-5.126420000	-0.085576000	-1.412615000
	50	1.939474000	-2.632438000	-0.576744000
	50	3.399052000	-1.466521000	-2.931436000
	50	-5.056828000	-0.672351000	1.505012000
	50	-3.516401000	2.453653000	-1.975915000
	50	-8.390587000	-0.303121000	-1.411155000
	50	3.047016000	2.080847000	0.344749000
	50	-8.319009000	-0.901815000	1.570756000
	50	-10.220213000	-3.112672000	2.166800000
	50	-11.827820000	-0.606645000	1.694077000
	50	-9.913242000	1.400437000	0.519531000
	50	-11.859723000	-3.011216000	-0.319748000
	50	-10.337436000	-2.130538000	-2.725590000
	50	-8.697818000	-3.274845000	-0.448424000
	50	-11.897929000	-0.015552000	-1.249404000

	50	-1.489697000	-0.314797000	1.509876000
	50	1.560581000	-0.279039000	1.442089000
	50	5.126420000	0.085576000	1.412615000
	50	5.071307000	-2.316430000	-0.587936000
	50	-1.939474000	2.632438000	0.576744000
	50	-3.399052000	1.466521000	2.931436000
	50	5.056828000	0.672351000	-1.505012000
	50	3.516401000	-2.453653000	1.975915000
	50	8.390587000	0.303121000	1.411155000
	50	-3.047016000	-2.080847000	-0.344749000
	50	8.319009000	0.901815000	-1.570756000
	50	10.220213000	3.112672000	-2.166800000
	50	11.827820000	0.606645000	-1.694077000
	50	9.913242000	-1.400437000	-0.519531000
	50	11.859723000	3.011216000	0.319748000
	50	10.337436000	2.130538000	2.725590000
	50	8.697818000	3.274845000	0.448424000
	50	11.897929000	0.015552000	1.249404000
Sn_{36}^{8-}	Level of theory: PBE0/def2-TZVP + D3 correction			
	50	-10.868671000	-4.536525000	-1.736413000
	50	-11.744797000	-3.060718000	0.890815000
	50	-10.322303000	-5.859057000	0.897067000
	50	-10.622942000	-1.541028000	-1.415996000
	50	-8.112783000	-5.634720000	-1.153905000
	50	-9.717922000	-3.742622000	2.968158000
	50	-7.877496000	-2.670398000	-1.443436000
	50	-9.043477000	-1.393990000	1.170324000
	50	-7.325491000	-4.015417000	1.230964000
	50	-4.943571000	-1.362152000	-1.356222000
	50	-3.513902000	-4.141626000	-1.353445000
	50	-4.399589000	-2.678678000	1.263307000
	50	-2.685659000	-2.012029000	-3.305750000
	50	-1.630443000	-0.006755000	-1.385366000
	50	1.080858000	1.340099000	-1.266073000
	50	1.770758000	4.223392000	-1.092834000
	50	0.588767000	2.951348000	1.363916000
	50	3.580618000	-0.264998000	-0.874083000
	50	10.868671000	4.536525000	1.736413000
	50	11.744797000	3.060718000	-0.890815000
	50	10.322303000	5.859057000	-0.897067000
	50	10.622942000	1.541028000	1.415996000
	50	8.112783000	5.634720000	1.153905000
	50	9.717922000	3.742622000	-2.968158000
	50	7.877496000	2.670398000	1.443436000
	50	9.043477000	1.393990000	-1.170324000

	50	7.325491000	4.015417000	-1.230964000
	50	4.943571000	1.362152000	1.356222000
	50	3.513902000	4.141626000	1.353445000
	50	4.399589000	2.678678000	-1.263307000
	50	2.685659000	2.012029000	3.305750000
	50	1.630443000	0.006755000	1.385366000
	50	-1.080858000	-1.340099000	1.266073000
	50	-1.770758000	-4.223392000	1.092834000
	50	-0.588767000	-2.951348000	-1.363916000
	50	-3.580618000	0.264998000	0.874083000

Supplemental References

1 Alvarez E, Grirrane A and Resa I *et al*. *Angew Chem Int Ed* 2007; **46**: 1296-1299.
2. Sheldrick GM. *Acta Crystallogr Sect A: Found Adv* 2015; **71**: 3-8.
3. Dolomanov OV, Bourhis LJ and Gildea RJ *et al*. *J Appl Crystallogr* 2009; **42**: 339-341.
4. Spek AL. *Acta Crystallogr, Sect D: Biol Crystallogr* 2009; **65**: 148-155.
5. Spek AL. Acta Crystallogr Sect C *Cryst Struct Commun* 2015; **71**: 9-18.
6. Adamo C and Barone V. *J Chem Phys* 1999; **110**: 6158–6170.
7. Schäfer A, Huber C and Ahlrichs R. *J Chem Phys* 1994; **100**: 5829–5835.
8. Frisch, M. J. et al. Gaussian 16, Revision B.01, Gaussian, Inc., Wallingford CT, 2016.
9. Zubarev DY and Boldyrev AI. *Phys Chem Chem Phys* 2008; **10**: 5207-5217.
10. Tkachenko NV and Boldyrev AI. *Phys Chem Chem Phys* 2019; **21**: 9590-9596.
11. Silvi B and Savin A. *Nature*, 1994; **371**: 683–686.
12. Lu T and Chen F. *J Comput Chem* 2012; **33**: 580–592.
13. Amsterdam Density Functional (ADF 2019) Code, Vrije Universiteit: Amsterdam, The Netherlands. Available at: http://www.scm.com
14. Perdew JP, Burke K and Ernzerhof M. *Phys Rev Lett* 1996; **77**: 3865-3868.
15. Islas R, Heine T and Merino G. *Acc Chem Res* 2012; **45**: 215–228.
16. Merino G, Heine T and Seifert G. *Chem – A Eur J* 2004; **10**: 4367-4371.
17. Heine T, Corminboeuf C and Seifert G. *Chem Rev* 2005; **105**: 3889–3910.
18. Perdew JP, Burke K and Wang Y. *Phys Rev B* 1996; **54**: 16533–16539.
19. Handy NC and Cohen AJ. *Mol Phys* 2001; **99**: 403–412.
20. Baranac-Stojanović M. *RSC Adv* 2014; **4**: 308–321.
21. Klod S and Kleinpeter E. *J Chem Soc Perkin Trans* 2001; **2**: 1893–1898.
22. Charistos ND, Papadopoulos AG and Sigalas MP. *J Phys Chem A* 2014; **118**: 1113–1122.
23. Lenthe EV, Baerends EJ and Snijders JG. *J Chem Phys* 1994; **101**: 9783–9792.
24. Burgun A, Ellis BG and Roisnel T *et al*. *J Am Chem Soc* 2014; **16**: 4209-4219.
25. Noodleman L and Jr. JGN. *J Chem Phys* 1979; **70**: 4903-4906.
26. Ugrinov A. and Sevov S. C. *J. Am. Chem. Soc.,* 2002, **124**, 10990-10991.
27. Ugrinov A. and Sevov S. C. *Inorg. Chem.,* 2003, **42**, 5789-5791.

28. Wiberg K. B. *Tetrahedron*, 1968, **24**, 1083-1096.
29. Bader R. F. W. *Chem. Rev.,* 1991, **91**, 893-928.